ENHANCED ULTRASOUND IMAGE RECONSTRUCTION USING A COMPRESSIVE BLIND DECONVOLUTION APPROACH

Zhouye Chen[1,2] *Adrian Basarab*[1] *Denis Kouamé*[1]

[1] IRIT UMR CNRS 5505, University of Toulouse, Toulouse, France
[2]Institute of Sensors, Signals & Systems, Heriot-Watt University, Edinburgh EH14 4AS, UK

ABSTRACT

Compressive deconvolution, combining compressive sampling and image deconvolution, represents an interesting possibility to reconstruct enhanced ultrasound images from compressed measurements. The model of compressive deconvolution includes, in addition to the measurement matrix, a 2D convolution operator carrying the information on the system point spread function which is usually unkown in practice. In this paper, we propose a novel alternating minimization-based optimization scheme to invert the resulting linear model, to jointly reconstruct enhanced ultrasound images and estimate the point spread function. The performance of the method is evaluated on both Shepp-Logan phantom and simulated ultrasound data.

***Index Terms*—** Ultrasound imaging, Compressive sampling, Blind deconvolution, Alternating minimization

1. INTRODUCTION

With the possibility of increasing the frame rate and/or reducing the acquired data volume, the topic of compressive sampling (CS) in the field of ultrasound (US) imaging has attracted a growing interest from several research groups [1–6]. According to the CS theory, the reconstruction of US images from compressed measurements is possible provided two conditions are met: i) the image must have a sparse representation in a known basis or frame and ii) the measurement and sparsifying basis must be incoherent [7]. It has been thus shown that the radiofrequency (RF) data may be recovered based on its sparse representation in basis such as wavelets [5], waveatoms [8], 2D Fourier transform [2] or learned dictionaries [6], considering Bernoulli Gaussian [9] or α-stable statistical assumptions [10] and using various acquisition schemes such as plane-waves [5], Xampling [3] or projections on Gaussian [1] or Bernoulli random vectors [2].

Despite the promising results, the application of CS in US imaging still remains challenging. First, because of the specific ultrasound noise (speckle) and given that the two conditions mentioned above cannot be always strictly satisfied in practical situations. The images reconstructed through CS are usually less good in terms of signal to noise ratio compared to standard acquisitions, especially when the ratio between the number of linear measurements and the number of image samples in the image to be reconstructed (denoted as CS ration below) is low. Second, the quality of the reconstructed images is at most equivalent to those acquired using standard schemes whereas it is well-known that the spatial resolution, the signal-to-noise ratio and the contrast of standard US images are affected by the limited bandwidth of the imaging transducer, the physical phenomena related to US wave propagation such as diffraction and the imaging system.

In order to overcome these issues, we have recently proposed a compressive deconvolution (CD) framework aiming at reconstructing enhanced RF images from compressed linear measurements [11]. The main idea behind CD is to combine CS and deconvolution reconstructions leading to the following linear model:

$$\boldsymbol{y} = \Phi H \boldsymbol{x} + \boldsymbol{n} \tag{1}$$

where $\boldsymbol{y} \in \mathbb{R}^M$ contains M linear measurements obtained by projecting one RF image $H\boldsymbol{x} \in \mathbb{R}^N$ onto the CS acquisition matrix $\Phi \in \mathbb{R}^{M \times N}$, with $M << N$. $H \in \mathbb{R}^{N \times N}$ is a block circulant with circulant block (BCCB) matrix modelling the 2D convolution between the US system 2D point spread function (PSF) of the US system and the tissue reflectivity function (TRF) $\boldsymbol{x} \in \mathbb{R}^N$ (the desired image). Finally, $\boldsymbol{n} \in \mathbb{R}^M$ stands for a zero-mean additive white Gaussian noise. All the images in (1) are expressed in the standard lexicographical order.

We should note that similar models have been proposed for general image processing purpose [12–15] including a theoretical derivation of Restricted Isometry Property (RIP) for random mask imaging [16]. Nevertheless, in contrast to the solutions provided by these existing works, we formulated in [11] the reconstruction process into a constrained optimization problem exploiting the relationship between CS recovery and deconvolution. This algorithm in [11] based on alternating direction method of multipliers (ADMM) was further improved with faster convergence based on simultaneous direction method of multipliers (SDMM) in [17]. Both algorithms have achieved promising results with the assumption that the PSF was known or could be estimated in a pre-processing

step.

In this paper, we propose a compressive blind deconvolution (CBD) algorithm that processes simultaneously image reconstruction and PSF estimation. The remainder of the paper is organized as follows. In section 2 we formulate the compressive blind deconvolution problem. Section 3 details the proposed CBD algorithm. Simulation results are provided in section 4 before drawing the conclusions in section 5.

2. PROBLEM FORMULATION

Inspired by the existing joint identification methods for blind deconvolution problem [18–20] and the *prior* information on the PSF adopted in [21–23], we formulate the compressive blind deconvolution problem as below.

$$\begin{aligned}\min_{\boldsymbol{x}\in\mathbb{R}^N,\boldsymbol{a}\in\mathbb{R}^N,\boldsymbol{h}\in\mathbb{R}^s} & \parallel \boldsymbol{a} \parallel_1 +\alpha P(\boldsymbol{x})+\gamma \parallel \boldsymbol{h} \parallel_2^2 \\ & +\frac{1}{2\mu}\parallel \boldsymbol{y}-\Phi\Psi\boldsymbol{a} \parallel_2^2 \quad s.t. \quad H\boldsymbol{x}=\Psi\boldsymbol{a}\end{aligned} \tag{2}$$

where α, γ, μ are hyper-parameters weighting the different regularization terms and $\boldsymbol{h} \in \mathbb{R}^s$ represents the PSF with a support of size s. The objective function in (2) contains, in addition to the data fidelity term, three regularization terms. The first term aims at imposing the sparsity of the RF data $H\boldsymbol{x}$ in a transformed domain Ψ. The second term $P(\boldsymbol{x})$ represents the *a priori* information of the target image (TRF) $\boldsymbol{x}$. We employed an ℓ_p-norm (adapted to US images) where the parameter p ($1 \leq p \leq 2$) is related to the generalized Gaussian distribution (GGD) modelling US images [24, 25]. This allows us to generalize the existing works in US image deconvolution mainly based on Laplacian or Gaussian statistics [18, 26]. A CD approach using a generalized total variation (TV) regularization has also been detailed in [11] and will also be used herein for comparison purpose with the existing CBD method in [15]. The third term (ℓ_2-norm) serves to regularize the PSF [21–23].

Unlike the CD problem in [11], this objective function is no longer convex. We hereafter present a dedicated algorithm to solve this optimization problem.

3. PROPOSED ALGORITHM

The aforementioned objective function in (2) can be divided into two sub-problems by an the alternating minimization (AM)-based algorithm, see, e.g., [27]. The first sub-problem, aiming at estimating $\boldsymbol{a}$ and $\boldsymbol{x}$ for a fixed $\boldsymbol{h}$ at kth iteration, can be written as:

$$\begin{aligned}(\boldsymbol{x}^{k+1},\boldsymbol{a}^{k+1}) = \underset{\boldsymbol{x}\in\mathbb{R}^N,\boldsymbol{a}\in\mathbb{R}^N}{argmin} & \parallel \boldsymbol{a} \parallel_1 +\alpha P(\boldsymbol{x}) \\ & +\frac{1}{2\mu}\parallel \boldsymbol{y}-\Phi\Psi\boldsymbol{a} \parallel_2^2 \quad s.t. \quad H^k\boldsymbol{x}=\Psi\boldsymbol{a}\end{aligned} \tag{3}$$

This sub-problem corresponds to the non-blind CD problem that we have previously solved in [11, 17]. Both the ADMM-based and SDMM-based algorithms in [11, 17] are able to estimate $\boldsymbol{x}^{k+1}$ and $\boldsymbol{a}^{k+1}$ at the same time.

The second sub-problem concerns the estimation of $\boldsymbol{h}$ for fixed $\boldsymbol{a}$ and $\boldsymbol{x}$:

$$\boldsymbol{h}^{k+1} = \underset{\boldsymbol{h}\in\mathbb{R}^s}{argmin} \quad \gamma \parallel \boldsymbol{h} \parallel_2^2 \quad s.t. \quad X^{k+1}P\boldsymbol{h}=\Psi\boldsymbol{a}^{k+1} \tag{4}$$

where $X^{k+1} \in \mathbb{R}^{N\times N}$ is a Block Circulant with Circulant Block (BCCB) matrix with the same structure as H. Its circulant kernel is $\boldsymbol{x}^{k+1} \in \mathbb{R}^N$. $P \in \mathbb{R}^{N\times s}$ is a simple structure matrix mapping the s coefficients of the PSF kernel $\boldsymbol{h}$ to a N length vector so that $H\boldsymbol{x}^{k+1} = X^{k+1}P\boldsymbol{h}$, see, e.g., [28]. The constrained problem above can be solved by reformulating it as an unconstrained one, thus becoming a regularized least square problem. Its analytical solution has been given in [21]:

$$\boldsymbol{h}^{k+1} = [(X^{k+1}P)^t X^{k+1}P+\gamma I_s]^{-1}(X^{k+1}P)^t\Psi\boldsymbol{a}^{k+1} \tag{5}$$

where $I_s \in \mathbb{R}^s$ is an identity matrix. We notice that instead of inverting an $N \times N$ matrix, we hereby only need to deal with the inversion of an $s \times s$ matrix. The computational cost is thus reduced. More details about the practical implementation of the analytic solution in (5) can be found in [28].

The proposed AM-based algorithm for CBD is summarized in Algorithm 1.

Algorithm 1 AM-based compressive blind deconvolution algorithm.

Input: $\boldsymbol{h}^0$, α, μ, β, γ

1: **while** not converged **do**
2: $\quad \boldsymbol{x}^{k+1}, \boldsymbol{a}^{k+1} \leftarrow \boldsymbol{h}^k$ ▷ update $\boldsymbol{x}^{k+1}$, $\boldsymbol{a}^{k+1}$ using ADMM-based [11] or SDMM-based [17] algorithms
3: $\quad \boldsymbol{h}^{k+1} \leftarrow \boldsymbol{x}^{k+1}, \boldsymbol{a}^{k+1}$ ▷ update $\boldsymbol{h}^{k+1}$ using (5)
4: **end while**

Output: $\boldsymbol{x}, \boldsymbol{a}, \boldsymbol{h}$

4. SIMULATION RESULTS

In this section, we provide a preliminary evaluation of the proposed CBD method's performance through two numerical experiments. The first simulation is based on the Shepp-Logan phantom and serves to compare our approach to the method in [15], referred as CBD_Amizic hereafter. Second, we test our algorithm on a simulated US image, showing the effectiveness of our approach compared to the compressive non-blind deconvolution method in [17].

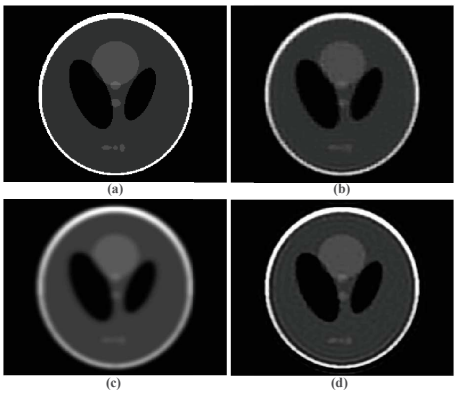

Fig. 1: Results on Shepp-logan phantom. (a) Original, (c) blurred, (b,d) reconstruction results respectively with CBD_Amizic and the proposed method for CS ratios of 0.4.

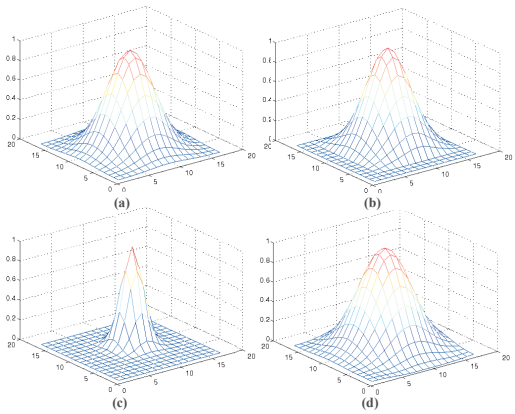

Fig. 2: Estimated PSFs for compressive blind deconvolution presented in Fig. 1. (a) Original, (c) initial, (b,d) estimated PSFs respectively with CBD_Amizic and the proposed method for CS ratios of 0.4.

4.1. Results on Shepp-logan phantom

The comparison results in this subsection are obtained on the standard 256×256 Shepp-Logan phantom. For fair comparison, the measurements have been generated in a similar manner as in [15], *i.e.* the original image was normalized, degraded by a 17×17 Gaussian PSF with variance of 9 and projected onto a structured random matrix (SRM) to generate the CS measurements. Finally, the compressed measurements were corrupted by an additive Gaussian noise corresponding to a SNR of 40 dB. We should remark that in [15] the compressed measurements were originally generated using a Gaussian random matrix. However, we have found that the reconstruction results with CBD_Amizic are slightly better when using a SRM compared to the PSNR (Peak Signal-to-Noise Ratio) results reported in [15]. Both methods used the generalized TV to regularize the reconstructed image and the 3-level Haar wavelet transform as sparsifying basis Ψ. With our method, the ADMM-based approach in [11] was employed to update $\boldsymbol{x}$ and $\boldsymbol{a}$. All the hyperparameters were manually set to their best possible values by cross-validation and both algorithms used the same stopping criteria.

Table 1: Quantitative assessment for Shepp-Logan phantom

Methods	CS ratios	PSNRx	PSNRh	Time/s
CBD_Amizic	80%	22.55	86.86	353.64
	60%	22.48	86.49	415.96
	40%	22.38	86.18	535.59
	20%	19.80	82.41	534.34
Proposed	80%	**24.39**	**92.41**	**243.31**
	60%	**23.12**	**89.70**	**320.82**
	40%	**22.59**	**88.36**	**321.39**
	20%	**21.48**	**85.96**	**329.90**

Fig. 1 shows the original Shepp-Logan image, its blurred version and a series of compressive deconvolution reconstructions using both our method and CBD_Amizic, for a CS ratio of 0.4. Additionally, in Fig. 2, we provided the estimated PSFs together with the true Gaussian PSF of variance 9 used to degrade the original images and the initial Gaussian PSF of variance 2 as used in [15]. Table 1 regroups the PSNR of the estimated $\boldsymbol{x}$ and $\boldsymbol{h}$ obtained with our method and with CBD_Amizic for four CS ratios ranging from 0.2 to 0.8. In each case, the reported PSNRs are the mean values of 10 experiments. We may observe that our method outperforms CBD_Amizic in all the cases. Moreover, our approach is less time consuming than CBD_Amizic for all the CS ratios considered[1]. Both algorithms were implemented using Matlab on a standard desktop computer (Intel Xeon CPU E5620 @ 2.40GHz, 4.00G RAM).

4.2. Results on simulated US images

In this section, we tested the proposed method on one simulated US image. Given that the CBD_Amizic method using a generalized TV prior is not well-suited to model the TRF in US imaging (see [11]), we did not use it in the following simulation.

This initial investigation uses an US image generated by 2D convolution between a spatially invariant Gaussian PSF of variance 2 and a TRF, shown in Fig. 3(a)(e). The TRF corresponds to a simple medium representing a round hypoechoic inclusion into a homogeneous medium. The scatterer amplitudes were random variables distributed according to a GGD with the shape parameter equal to 1.5. The compressed measurements were obtained by projecting the RF images onto a

[1]For CBD_Amizic method, we used the original code provided by the authors of [15].

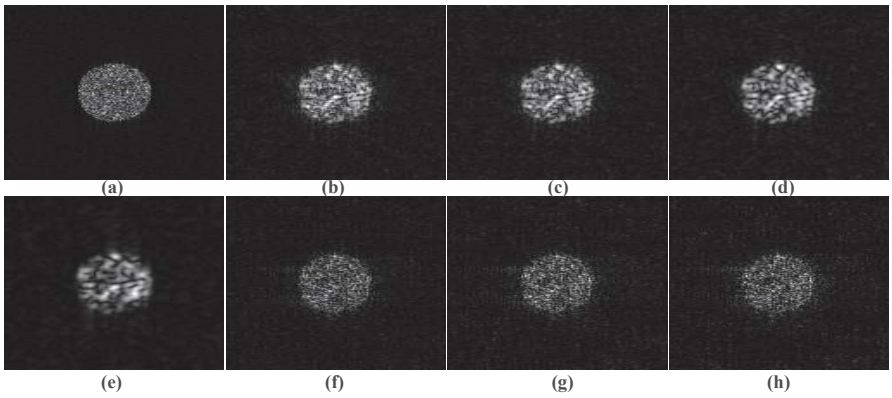

Fig. 3: Simulated US image and its reconstruction results for a SNR of 40 dB. (a) TRF, (e) Simulated B-mode US image, (b,c,d) results using CD algorithm with a pre-estimated PSF for CS ratios of 0.8, 0.6 and 0.4, (f,g,h) results using proposed method for CS ratios of 0.8, 0.6 and 0.4.

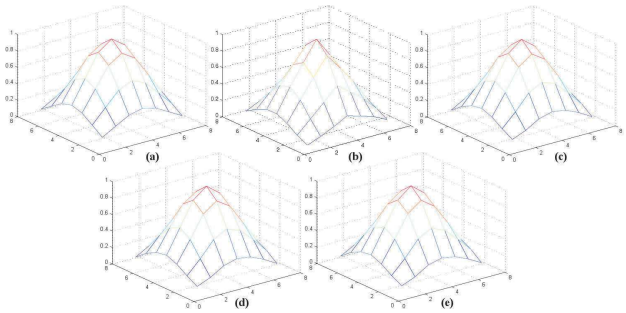

Fig. 4: Estimated PSFs for compressive blind deconvolution presented in Fig. 3. (a) True PSF, (b) initial PSF (estimated using an exiting method [29]), (c,d,e) estimated PSF with proposed method for CS ratios of 0.8, 0.6 and 0.4.

Table 2: Quantitative assessment for simulated US data

Methods	CS ratios	PSNRx	PSNRh
CD_true	80%	26.86	-
	60%	25.38	
	40%	24.75	
	20%	22.74	
CD	80%	20.47	23.20
	60%	20.07	
	40%	19.61	
	20%	18.82	
Proposed	80%	**23.51**	**26.73**
	60%	**23.20**	**26.35**
	40%	**22.30**	**25.30**
	20%	**20.80**	**23.34**

SRM, aiming at reducing the amount of data available.

The proposed method was compared to the non-blind CD algorithm in [17]. With the non-blind approach, the PSF was pre-estimated from the blurred data following the PSF estimation procedure presented in [29]. The proposed method takes this PSF as an initial guess and updates it iteratively. The true and estimated PSFs are shown in Fig. 4, while the reconstructed images are regrouped in Fig. 3. In order to give an upper bound to the results, we provided also the results of CD algorithm with the true PSF, denoted by CD_true in Table 2. The visual inspection and the quantitative results in Table 2 confirm that the proposed method is able to recover both TRF and PSF with better accuracy that the non-blind approach.

5. CONCLUSION

This paper presents an initial investigation of a compressive blind deconvolution algorithm. The proposed AM-based approach iteratively alternates between on the one hand, the estimation of the TRF and the sparse representation of the blurred US RF image, and on the other hand the PSF update solved analytically. Simulation results on the standard Shepp-Logan phantom show the superiority of our method, both in accuracy and in computational time, over an existing compressive blind deconvolution approach [15]. Finally, preliminary results on a simulated US image have also shown the efficiency of the proposed approach on both TRF and PSF estimation over a non-blind approach. Our future work will mainly focus on a further evaluation of the proposed algorithm, both on simulated and experimental data. The interest of other PSF regularization functions will be also investigated.

References

[1] Alin Achim, Benjamin Buxton, George Tzagkarakis, and Panagiotis Tsakalides, "Compressive sensing for ultrasound rf echoes using a-stable distributions," in *Engineering in Medicine and Biology Society (EMBC), 2010 Annual International Conference of the IEEE*. IEEE, 2010, pp. 4304–4307.

[2] Céline Quinsac, Adrian Basarab, and Denis Kouamé, "Frequency domain compressive sampling for ultrasound imaging," *Advances in Acoustics and Vibration, Advances in Acoustic Sensing, Imaging, and Signal Processing*, vol. 12, pp. 1–16, 2012.

[3] Tanya Chernyakova and Yonina Eldar, "Fourier-domain beamforming: the path to compressed ultrasound imaging," *Ultrasonics, Ferroelectrics, and Frequency Control, IEEE Transactions on*, vol. 61, no. 8, pp. 1252–1267, 2014.

[4] Hervé Liebgott, Adrian Basarab, Kouameé Denis, Olivier Bernard, and Denis Friboulet, "Compressive sensing in medical ultrasound," in *2012 IEEE International Ultrasonics Symposium*. IEEE, 2012, pp. 1–6.

[5] Martin F Schiffner and Georg Schmitz, "Fast pulse-echo ultrasound imaging employing compressive sensing," in *Ultrasonics Symposium (IUS), 2011 IEEE International*. IEEE, 2011, pp. 688–691.

[6] Oana Lorintiu, Hervé Liebgott, Martino Alessandrini, Olivier Bernard, and Denis Friboulet, "Compressed sensing reconstruction of 3d ultrasound data using dictionary learning and line-wise subsampling," *Medical Imaging, IEEE Transactions on*, vol. 34, no. 12, pp. 2467–2477, 2015.

[7] Emmanuel J Candès and Michael B Wakin, "An introduction to compressive sampling," *Signal Processing Magazine, IEEE*, vol. 25, no. 2, pp. 21–30, 2008.

[8] Hervé Liebgott, Rémy Prost, and Denis Friboulet, "Pre-beamformed rf signal reconstruction in medical ultrasound using compressive sensing," *Ultrasonics*, vol. 53, no. 2, pp. 525–533, 2013.

[9] Nicolas Dobigeon, Adrian Basarab, Denis Kouamé, and Jean-Yves Tourneret, "Regularized Bayesian compressed sensing in ultrasound imaging (regular paper)," in *European Signal and Image Processing Conference (EUSIPCO), Bucharest, Romania, 27/08/2012-31/08/2012*, http://www.eurasip.org/, août 2012, pp. 2600–2604, EURASIP.

[10] Alin Achim, Adrian Basarab, George Tzagkarakis, Panagiotis Tsakalides, and Denis Kouamé, "Reconstruction of ultrasound RF echoes modelled as stable random variables," *IEEE Transactions on Computational Imaging*, vol. 1, no. 2, pp. 86–95, juin 2015.

[11] Zhouye Chen, Adrian Basarab, and Denis Kouamé, "Compressive deconvolution in medical ultrasound imaging," *IEEE transactions on medical imaging*, vol. 35, no. 3, pp. 728–737, 2016.

[12] Jianwei Ma and Francois-Xavier Le Dimet, "Deblurring from highly incomplete measurements for remote sensing," *Geoscience and Remote Sensing, IEEE Transactions on*, vol. 47, no. 3, pp. 792–802, 2009.

[13] Liang Xiao, Jun Shao, Lili Huang, and Zhihui Wei, "Compounded regularization and fast algorithm for compressive sensing deconvolution," in *Image and Graphics (ICIG), 2011 Sixth International Conference on*. IEEE, 2011, pp. 616–621.

[14] Manqi Zhao and Venkatesh Saligrama, "On compressed blind deconvolution of filtered sparse processes," in *Acoustics Speech and Signal Processing (ICASSP), 2010 IEEE International Conference on*. IEEE, 2010, pp. 4038–4041.

[15] Bruno Amizic, Leonidas Spinoulas, Rafael Molina, and Aggelos K Katsaggelos, "Compressive blind image deconvolution," *Image Processing, IEEE Transactions on*, vol. 22, no. 10, pp. 3994–4006, 2013.

[16] Sohail Bahmani and Justin Romberg, "Compressive deconvolution in random mask imaging," *IEEE Transactions on Computational Imaging*, vol. 1, no. 4, pp. 236–246, 2015.

[17] Zhouye Chen, Adrian Basarab, and Denis Kouamé, "Reconstruction of Enhanced Ultrasound Images From Compressed Measurements Using Simultaneous Direction Method of Multipliers," *IEEE Transactions on Ultrasonics, Ferroelectrics and Frequency Control*, 2016.

[18] Oleg Michailovich and Allen Tannenbaum, "Blind deconvolution of medical ultrasound images: a parametric inverse filtering approach," *Image Processing, IEEE Transactions on*, vol. 16, no. 12, pp. 3005–3019, 2007.

[19] Mariana SC Almeida and Luis B Almeida, "Blind and semi-blind deblurring of natural images," *Image Processing, IEEE Transactions on*, vol. 19, no. 1, pp. 36–52, 2010.

[20] Chengpu Yu, Cishen Zhang, and Lihua Xie, "A blind deconvolution approach to ultrasound imaging," *Ultrasonics, Ferroelectrics, and Frequency Control, IEEE Transactions on*, vol. 59, no. 2, pp. 271–280, 2012.

[21] Renaud Morin, Stéphanie Bidon, Adrian Basarab, and Denis Kouamé, "Semi-blind deconvolution for resolution enhancement in ultrasound imaging," in *Image Processing (ICIP), 2013 20th IEEE International Conference on*. IEEE, 2013, pp. 1413–1417.

[22] Audrey Repetti, Mai Quyen Pham, Laurent Duval, Emilie Chouzenoux, and J-C Pesquet, "Euclid in a taxicab: Sparse blind deconvolution with smoothed regularization," *Signal Processing Letters, IEEE*, vol. 22, no. 5, pp. 539–543, 2015.

[23] Ningning Zhao, Adrian Basarab, Denis Kouamé, and Jean-Yves Tourneret, "Joint bayesian deconvolution and pointspread function estimation for ultrasound imaging," in *Biomedical Imaging (ISBI), 2015 IEEE 12th International Symposium on*. IEEE, 2015, pp. 235–238.

[24] Martino Alessandrini, Simona Maggio, Jonathan Porée, Luca De Marchi, Nicolo Speciale, Emilie Franceschini, Olivier Bernard, and Olivier Basset, "A restoration framework for ultrasonic tissue characterization," *Ultrasonics, Ferroelectrics, and Frequency Control, IEEE Transactions on*, vol. 58, no. 11, pp. 2344–2360, 2011.

[25] Ningning Zhao, Adrian Basarab, Denis Kouamé, and Jean-Yves Tourneret, "Joint Segmentation and Deconvolution of Ultrasound Images Using a Hierarchical Bayesian Model based on Generalized Gaussian Priors," *IEEE Transactions on Image Processing*, 2016.

[26] Torfinn Taxt and Jarle Strand, "Two-dimensional noise-robust blind deconvolution of ultrasound images," *Ultrasonics, Ferroelectrics, and Frequency Control, IEEE Transactions on*, vol. 48, no. 4, pp. 861–866, 2001.

[27] Yilun Wang, Junfeng Yang, Wotao Yin, and Yin Zhang, "A new alternating minimization algorithm for total variation image reconstruction," *SIAM Journal on Imaging Sciences*, vol. 1, no. 3, pp. 248–272, 2008.

[28] Renaud Morin, *Amélioration de la résolution en imagerie ultrasonore*, Thèse de doctorat, Université de Toulouse, Toulouse, France, novembre 2013, (Soutenance le 29/11/2013).

[29] Oleg V Michailovich and Dan Adam, "A novel approach to the 2-d blind deconvolution problem in medical ultrasound," *Medical Imaging, IEEE Transactions on*, vol. 24, no. 1, pp. 86–104, 2005.